Effect of thickness and cracking phenomena on the photocatalytic performances of Ti/TiO$_2$ photoanodes produced by dip coating

Lucio Scandola[a], Saverio Latorrata*[a], Roberto Matarrese[b], Cinzia Cristiani[a], Isabella Nova[b]

[a] Department of Chemistry, Materials and Chemical Engineering "Giulio Natta", Politecnico di Milano, piazza Leonardo da Vinci 32, 20133 Milan (Italy)

[b] Department of Energy, Politecnico di Milano, Via La Masa 34, 20156 Milan (Italy)

*e-mail: saverio.latorrata@polimi.it

Abstract

Photoanodes for water-splitting applications were produced by coating acid-treated Ti slabs using an aqueous dispersion of TiO_2, polyvinyl alcohol and glycerol. Such components were adjusted to achieve a lower viscosity at a 10 s^{-1} shear rate, considered as representative of the dip-coating application, for the sake of reducing the final coating thickness while increasing its quality.

A correlation was found between the thickness of the oxide layer and the percentage of area occupied by the crevices, which appeared, during the thermal treatment, as an effect of the liquid phase removal. Also, the adhesion appeared to be strongly related to the cracking phenomena, since less cracked samples withstood much lower weight losses during the adhesion tests.

The lower adhesion of thicker coatings was found to affect the photo-catalytic performances of the photoanodes, showing lower photocurrents and efficiencies when compared with thinner ones.

1. Introduction

The world's need for energy is growing with its population and most of this hunger is still fed using fossil fuels as oil, coal and natural gas. The expected future developments, as technology becomes even more invasive of every aspect of life, are of an even larger energy intake. Even if the non-renewable sources are, up to now, the larger energy source, representing the 80 % of the global consumption, a lot of research has been performed in the direction of the so called "clean fuels".

The 2017 International Energy Outlook reports the renewable energies as the world's fastest-growing energy source [1], with a rate of increase larger than the nuclear energy.

One of the main issues with the renewable power sources, taking solar energy as an example, is that their product needs to be used immediately or stored in a suitable way. Energy storage, indeed, is a crucial problem which leads to an extensive research in the fields of batteries and fuels that can stock the outcome of renewable power plants to use it at a later stage. One of the means that have been detected as candidates for the stocking process is hydrogen. The importance of hydrogen, it being an energy carrier, is strongly related to its production process.

Up to now, the 75 % of the hydrogen production is carried out using fossil sources mainly by steam methane reforming or, in smaller amounts, by water electrolysis [2].

Photo-electrochemical water-splitting is a hydrogen production method known since the 70's, and developed for the first time in the 1972 by Fujishima and Honda [3]. This application involves the use of a semiconductor with a suitable band structure to catalyze the water electrolysis. This process takes place in a photo-electrochemical cell (PEC) [4] which is essentially made of two electrodes, with one of them being coated with a photo-active material,

immersed in a water electrolyte solution and connected to a potentiostat, which is used to regulate the potential drop and to measure the generated current.

Usually the photo-active electrode is the anode [5] and it is made of a metallic support coated with a semiconductor. The choice for the semiconductor is not a trivial one, since it has to comply with some key properties in order to be effective as a photocatalyst, concerning its band structure, its stability in aqueous environments and its corrosion resistance [6-8]. The first semiconductor used by Fujishima and Honda [3] for this purpose was titanium dioxide, and it has become, during the years, the reference material of this particular field of application [9-14] due to its chemical stability, non-toxicity, high resistance to photocorrosion and low cost. Unfortunately, TiO_2 suffers from severe limitations, the two most important ones being the poor activation by visible light and the low overall efficiency which is affected by the high degree of recombination between the photogenerated charge carriers (electron-hole pairs). Accordingly, various approaches have been proposed to improve the PEC performance of TiO_2, such as TiO_2 doping/sensitization to shift the absorption from UV towards the visible light [15], and controlling photocatalyst structure and morphology to improve charge transport [16].

In the latter case, one way to increase the efficiency of a photoanode involves the deposition of a nanostructured coating in order to create a preferential pathway for the electrons, increasing the mean free path and preventing recombination phenomena [13, 17, 18]. Unfortunately, most of these applications, such as sputtering [19], chemical vapor deposition (CVD) [11] or pulsed laser deposition (PLD) [20], often require a very high technology level and a consequently high production cost [21].

This research work was focused on the study of a very cheap coating method which can be easily implemented in mass-production: dip coating [12, 22-25].

The main objective was to check if there was any room for improvement of samples produced using the aforementioned coating technique and to understand how the coating features, such as thickness, cracking, adhesion, could be relevant in the determination of its photocatalytic activity. Cracking phenomena are unavoidable when dealing with deposition of dispersed particles and can be detrimental and pronounced depending on the ratio of components in the slurry formulation and operating conditions of both coating and thermal treatment process. The number and the size of generated surface cracks is strongly influenced by thickness of the deposited layer which in turn can lead to better or worse adhesion.

We used a quantitative method, which consisted in post-processing of SEM images of the samples surfaces, to evaluate the entity of the cracks formed during the thermal treatment. To the best of our knowledge, there is no study in literature that analyzes how the cracking phenomena in thin films of TiO_2 can affect the photocatalytic performances. In this respect, this work does not want to be a further improvement on the state of the art of TiO_2 catalyzed water splitting, but tries to put a focus on a common issue [25-28] of dip-coated TiO_2 thin films and its effect in their photo-catalytic performances. The study focuses on the importance of reducing dynamic viscosity of particles dispersion in order to get a thinner and more adhering coating which would present a low content of cracks. Thus it is not related to a systematic analysis about the best composition needed to achieve the lowest viscosity, rather it has been intended as a preliminary attempt to investigate the effect of the coating features on photoelectrochemical performances.

2. Experimental

Photoanodes were produced by dip-coating of a metallic Ti substrate with TiO_2. 4 cm^2 Ti slabs were obtained by cutting Ti foils of 0.25 mm thickness (Sigma Aldrich). Slabs were etched in 20

ml of HCl 37 % w/w (Sigma Aldrich) at 35 °C for 4 hours [29]. After the treatment, the slabs were rinsed in deionized water to remove acid residues.

Ti slabs were coated with titanium dioxide (Degussa P25) with a composition corresponding to 70 % anatase and 30 % rutile, an average particle size lower than 25 nm and a surface area of 35-65 m^2/g (BET). Coating slurries were obtained according to an already developed procedure [30]. Briefly, polyvinyl alcohol (PVA) (Mowiol® 8-88, 67000 g·mol^{-1}, Sigma Aldrich) was dissolved in deionized water in a round bottom flask equipped with a Vigreux column and heated at 85 °C for 1 hour under continuous stirring. The obtained solution was cooled down to room temperature and, afterwards, glycerol (GLY) (Sigma Aldrich, 86-89 % w/w water solution), and TiO_2 powder were added. The slurry was transferred into a polyethylene flask, added with zirconia spheres as grinding bodies and milled using a ball mill for 4 hours (rotation rate: 50 rpm). Then, the mixture was de-foamed by adding small amount of ethanol.

Starting from the initial composition reported in Table 1 [30], different slurry formulations were studied by varying the glycerol content from 14.68 g to 5.51 g and the PVA from 1.48 g to 0.37 g. TiO_2 content and water, instead, were kept constant for all the formulations, equal to 5 g and 7.5 g, respectively.

Table 1. Recipe for the starting TiO_2 mixture.

GLY/TiO$_2$ [g/g]	H$_2$O/TiO$_2$ [g/g]	PVA/(H$_2$O+GLY) [% wt]	TiO$_2$ [g]	GLY [g]	H$_2$O [g]	PVA [g]
2.20	1.50	4	5	11.01	7.5	0.74

Slurries viscosity was measured using a rotational rheometer (Stresstech 550, Reologica Instruments). The stability dispersions was assessed using test tubes technique and checking if

solid settling or clarification has occurred at different time [31]. All the dispersions did not show any visible sign of sedimentation, even after 48 hours, the full duration of the tests.

The coating process was carried out using a home-made dip-coater. The withdrawal velocity was set to 10 cm/min and after deposition the sample was left in vertical position (15 min) to drain excess slurry.

Coated slabs were heat-treated according to the following procedure in order to remove organic species and to enhance mechanical and electronic inter-particle connectivity: from room temperature to 100 °C (1 °C/min, 1 hour of dwelling time), from 100 °C to 300 °C (3 °C/min, 1 hour of dwelling time) and from 300 °C to 400 °C (1 °C/min, 1 hour of dwelling time), which was considered an optimal temperature for such treatment upon performing thermogravimetric analyses (Supplementary Material, Fig. S1).

Etched Ti slabs and final samples were characterized by Scanning Electron Microscopy (SEM), using a Zeiss EVO 50 EP. Several images were taken to evaluate the quality of the coating surface as well as cracking phenomena; deposited layers thickness was detected and measured after sintering from cross-section images.

Coating adhesion was verified by ultrasound bath test according to references [30, 32]. SEM images were analyzed using an image processing software (ImageJ). A color threshold was imposed to discriminate the darker areas (crevices) from the lighter ones (solid film).

The PEC water splitting behavior of the TiO_2 photoanodes was investigated in KOH aqueous solution (0.1 M) with a three-electrode cell equipped with a flat quartz window (see experimental setup sketched in Fig. 1).
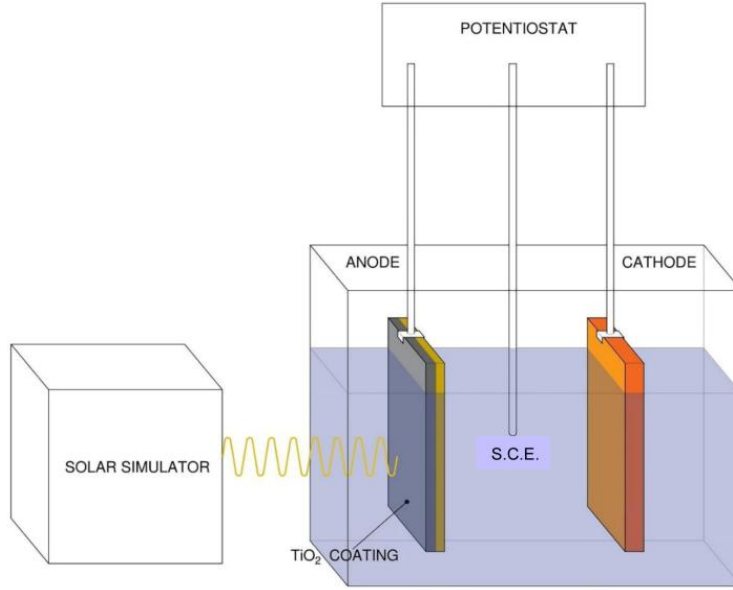
Fig. 1. Photo-electrochemical cell (PEC) setup used to test the sample.

Border inhomogeneity effects of the samples were masked with an insulating tape leaving a working area of 1 cm^2. A platinum grid and a saturated calomel electrode (SCE) were used as counter and reference electrode, respectively. A 300 W xenon arc lamp and AM1.5G filter (Lot Quantum Design LSZ389) were used as light source. A light intensity of 96000 μW cm^{-2} was measured, prior to the experiments, using a light meter HD2302.0 (Delta OHM). The performance of the TiO$_2$ photoanodes was evaluated by measuring photocurrents under an external bias [5, 33-35] provided by a potentiostat (Amel 7050) performing potential ramps from −0.8 V to about 0.5 V, with a scan rate of 5 mV/s.

The photocurrent results were used to calculate the photoconversion efficiency (η %) according to equation (1), which takes into account not only the power light, but also the external potential applied to the electrode [36, 37],

$$\eta \ (\%) = \frac{J(E^0 - |E_{app}|)}{I} \times 100 \quad (1)$$

where J is the photocurrent density (μWcm^{-2}), $E° =1.23$ V is the standard reversible potential for water splitting, $\lvert E_{app} \rvert$ is the external applied potential, evaluated as the difference between the measured potential (V) vs. SCE and the Open Circuit Voltage (OCV) under the irradiated power light, and I is the incident light power density.

3. Results and Discussion

3.1 Support pre-treatment

Support pre-treatment is required to favor coating adhesion [29]. Accordingly, slabs were treated in HCl for 4 hours at 35 °C and the effect of the etching was investigated by SEM analysis both in direct and backscattering mode. Images are compared in Fig. 2. It is evident that (Fig. 2a) in pristine Ti slabs only traces of manufacturing (e.g. lamination) are present. The surface is planar and quite homogeneous without cracks, holes or crevices. Upon treatment in HCl for 4 hours the formation of surface roughness occurred (Fig. 2b). This effect is expected to favor the contact between the support and the coating layer, thus improving TiO_2 adhesion. From a chemical point of view, we can refer to backscattering measurements (Fig. 2c), where the existence of a corrosion byproduct at the surface can be supposed.
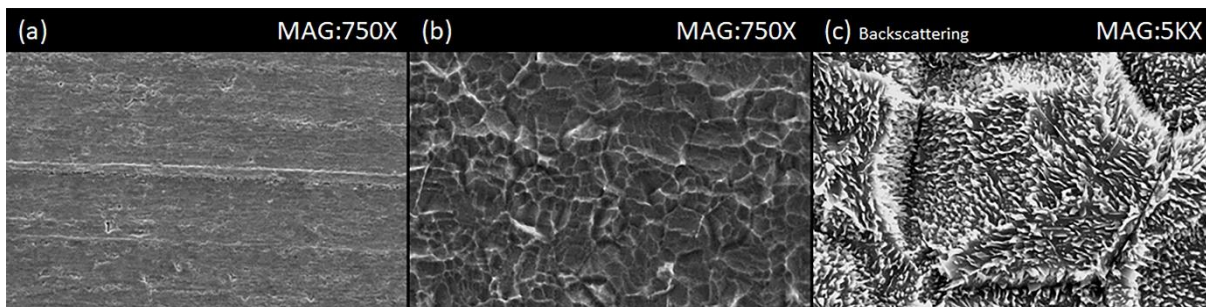
Fig. 2. SEM image of Ti slabs: a) untreated surface; b) upon 4 hours of HCl treatment and c) upon 4 hours of HCl treatment in backscattering mode.

We could not measure the potential of the whole system, so only a tentative hypothesis can be made about the nature of such product. Considering the experimental conditions and the Ti Pourbaix diagrams [39], it might be identified as both a titanium hydride or oxide, depending on the generated potential [38-40]. Anyway, the formation of an oxide layer is supposed to be more likely due to the low temperature used for the etching process (higher temperatures would lead to higher chances to form TiH_x [40]).

3.2 Slurry formulation

Slurry composition and stability are crucial when performing dip-coating, since the concentration of each component can modify the rheological behavior of the mixture, thus affecting the coating process.

The composition was selected on the basis of previous results obtained on slurry formulation for other ceramic oxides [41]. Moreover, the stability of the mixture was assessed through sedimentation tests, by filling a test tube and monitoring the eventual clarification of the upper part of the solution. No clarification was visible during sedimentation, even after 48 hours.

Therefore, it was concluded that slurries were stable enough and proper to be used in the coating deposition process.

Considering the final target, i.e. the achievement of homogeneous thin layers strongly bonded to the substrate, a study was carried out to pursue lower thicknesses by decreasing slurry viscosity, according to dip-coating theory [42]. Indeed, for Newtonian fluids, the Landau-Levich equation (Eq. 2) relates the thickness of the wet layers (h_0) deposited on a substrate by dip-coating to the viscosity and withdrawal velocity during deposition [42, 43]:

$$h_0 = c \frac{(\mu u)^{2/3}}{\gamma_{lv}^{1/6}(\rho g)^{1/2}} \tag{2}$$

where c is a proportionality constant related to the curvature of the dynamic meniscus, u the withdrawal velocity, g the gravitational constant, μ, γ_{lv} and ρ are the dynamic viscosity, the surface tension of the liquid-vapor interface and the density of the dispersion, respectively.

A similar relationship has been found in the literature also in case of non-Netwonian fluids [44]: the Landau-Levich equation has to be properly modified to model the phenomenon, but the proportionality is preserved. Accordingly, thinner layers can be obtained managing slurry viscosity.

The relationship between viscosity and deposited layer thickness is true for the "wet" layer. After the heat treatment the film thickness will decrease depending on the loading of solid particles, porosity and slurry composition. However, in this work the loading of TiO_2 was constant, therefore the change in thickness can be related to change in dispersant and rheology modulator.

From the experimental point of view, several slurries were prepared by modifying the starting composition (Table 2). Viscosity was tested with particular attention to the value corresponding at shear rate 10 s^{-1} which is indeed that of interest for the dip-coating application.

Table 2. Composition and corresponding viscosity at shear rate 10 s^{-1}.

Dispersion	GLY [g]	PVA [g]	GLY [wt %]	PVA [wt %]	TiO$_2$ [wt %]	W [wt %]	Viscosity at 10 s^{-1} [Pa·s]
Slurry 1	11.01	0.37	46.11	1.55	20.94	31.41	0.40
Slurry 2	11.01	0.74	45.40	3.05	20.62	30.93	0.74
Slurry 3	11.01	1.11	44.72	4.51	20.31	30.46	3.93
Slurry 4	11.01	1.48	44.06	5.92	20.01	30.01	4.14
Slurry 5	5.51	0.52	29.74	2.81	26.98	40.47	1.76
Slurry 6	7.34	0.59	35.93	2.89	24.47	36.71	0.25
Slurry 7	14.68	0.89	52.30	3.17	17.81	26.72	0.72

Albeit preliminary, some significant results were found and a rough rheology-composition correlation was found, mainly due to PVA and glycerol content, being water/TiO$_2$ ratio fixed at 1.5 for all the samples. Glycerol and PVA, necessary to obtain dispersion of the powder and a stable slurry, exert two different effects, i.e. once fixed glycerol, addition of PVA increases viscosity (please compare slurries at constant GLY, Table 2), while the effect of glycerol cannot be assessed precisely with the performed tests or directly correlated to rheology, but it seems that a higher amount of such compound does not result in a corresponding high viscosity. Indeed, PVA acts as a rheology modulator while glycerol has been used as a dispersant for steric stabilization. Therefore, the final rheological behavior is the combination of these effects. Due to slurry complexity, it appears very challenging to design a model of the phenomena which contribute to the achievement of the final rheological behavior of the slurry. Considering only data here reported it is hard to rule out a clear relationship: a larger and deeper work has to be done that is out of scope of this preliminary investigation. Based on the data in Table 2, the most proper slurry was apparently Slurry 6, whose viscosity at a shear rate of 10 s^{-1} was 0.25 (Pa·s),

i.e. the lowest obtained with the compositions here reported. It seems that a threshold limit value for PVA does exist over that a sharp increase of viscosity happens. Indeed, for Slurry 6, PVA percentage stays below that limit (the one of Slurry 3), glycerol is reduced with respect to slurries showing a higher viscosity and water weight percentage is higher, which can result in a decrease of viscosity.

Anyway, to verify if the expected viscosity-thickness correlation was true also for these slurry compositions, viscosity at a 10 s^{-1} shear rate and final layer thickness were plotted in Fig. 3.
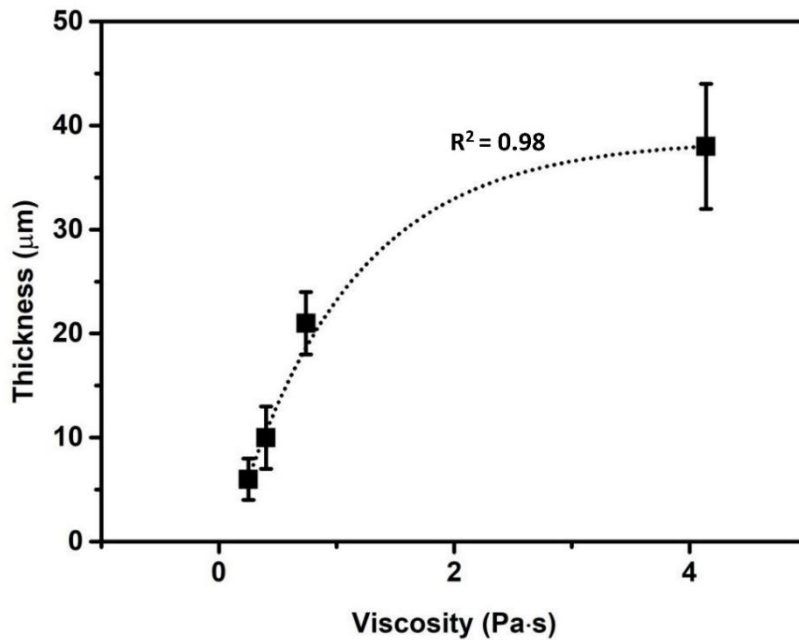

Fig. 3. Layer thickness as function of the slurry viscosity. The data have been fitted using a y=1/exp(x) curve.

It is evident that lower viscosity results in lower thickness. Layer thickness increases very quickly with viscosity increase in the range 0.2-1 Pa·s, suggesting that a strong influence of rheology is present for slurries with these compositions. On increasing viscosity, thickness apparently tends to reach a plateau value where viscosity influence is decreased and very thick coatings are obtained.

The other parameter to be accounted for Landau-Levich model, i.e. withdrawal velocity, was found to exert a very low influence: a thickness increase of 2 ± 1 μm (i.e. from roughly 10 μm up to about 12 μm) was observed by doubling the withdrawal velocity (i.e from 10 cm/min to 20 cm/min), as shown in Supplementary Material (Fig. S2). According to literature findings [30], it seems that tuning the blend composition is the most effective way of controlling the final coating thickness.

3.3 Coating

The coating deposition was carried out using the procedure described in the experimental section. Subsequently the samples were thermally treated to consolidate the TiO_2 layer and to eliminate the other reactants. The intrinsic issue to be dealt with, when drying a liquid film, is cracking. This cracking phenomenon is often referred as "mud-cracking" and it is caused by the capillary forces due to the evaporation of the liquid phase from inside the powder bed [45-47]. Being the cracking phenomenon related to the amount of liquid to be evolved, a relation can be expressed, through an energy balance and the use of Griffith's fracture mechanics, which links the cracks arising to a critical value of the humid film thickness [46].
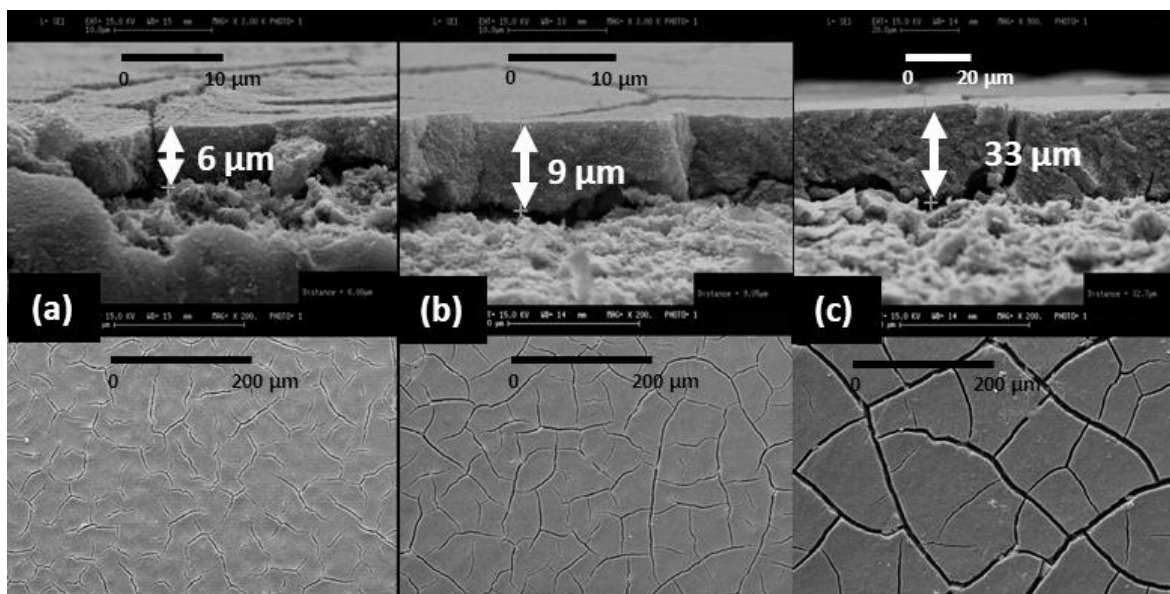
Fig. 4. SEM images showing surface cracks belonging to photoanodes with different thickness: (a) 6 μm, (b) 9 μm, (c) 33 μm.

SEM characterization was performed on the surfaces of final specimens with different thickness and a clear difference in cracks dimension and cracking extension was detected (Fig. 4). The surfaces were analyzed by means of an image processing program (ImageJ): a color threshold was imposed on several images of the coated oxide layers in order to detect the percentage of area occupied by the crevices (darker zones). This last value was plotted as a function of layer thickness (Fig. 5).
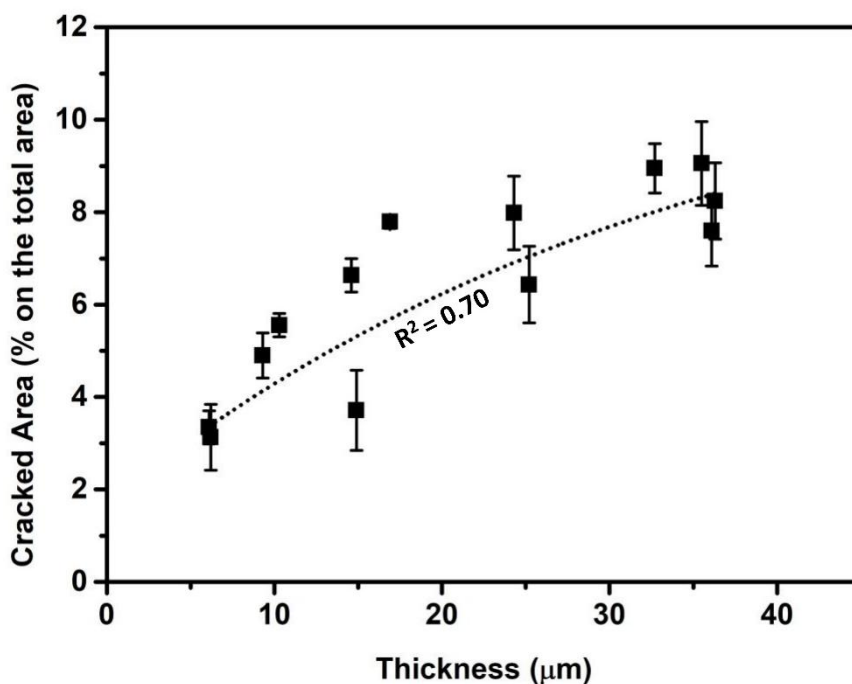
Fig. 5. Percentage of area occupied by the crevices as a function of the photo-catalytic layer thickness. The data have been fitted using a y=1/exp(x) curve.

The graph clearly states that the thicker the coating, the more relevant the cracking phenomena are. Such a delamination of the surface, due to the rapid evaporation of the solvent, could lead to a worse adhesion of the layer. A bad adhesion of the layer to the substrate could result in a worse electrical contact between the two photoanode components, thus worsening the photo-electrochemical performance of the material. To better analyze this phenomenon, adhesion tests were performed on the coated specimens; results are reported in Fig. 6, where images of the real coating, before and after adhesion test, are displayed.
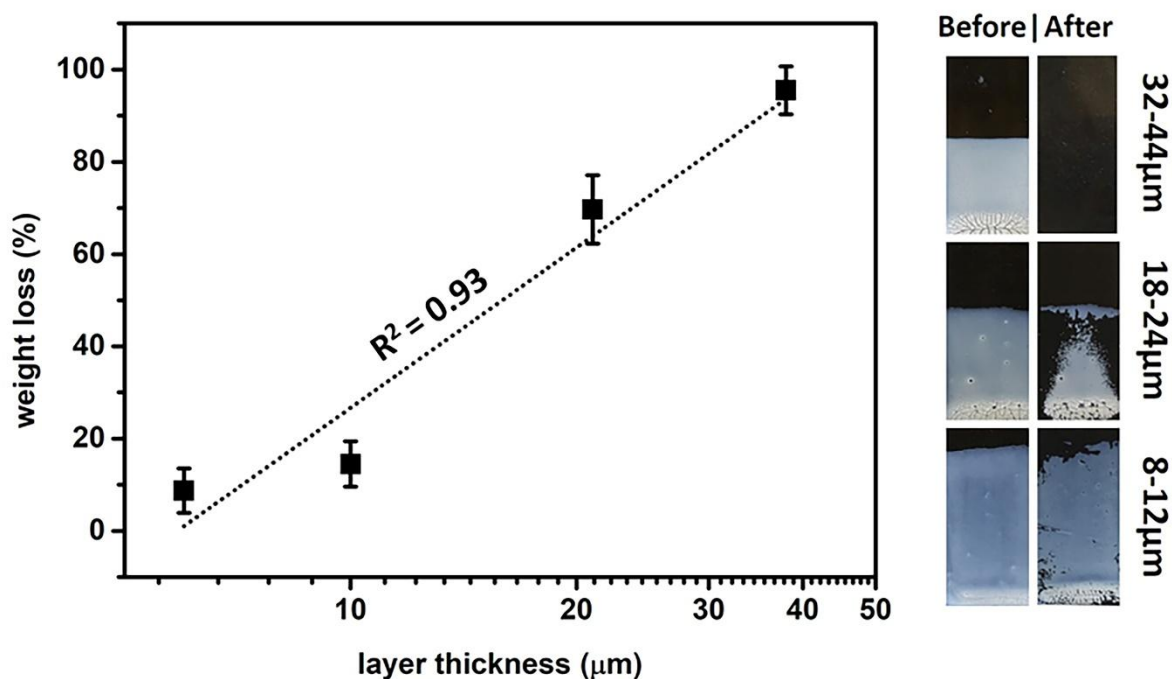
Fig. 6. Weight loss percentage upon adhesion test as a function of the coating layer thickness (left); Images of the samples before and after the adhesion tests (right).

A linear correlation was found between weight loss and layer thickness, i.e. cracking phenomena. Thinner, thus less cracked coated layers, could resist better the sonication, showing lower weight losses. This reflected in a higher quality, more homogeneous surface of the final coating that, being able to resist to the intense stress effects of the sonication process, confirmed its strong adhesion to the substrate. Such samples were those of choice for the photocatalytic application.

3.4 Photo-electrochemical tests

The photo-electrochemical activity of selected samples, reported in Table 3, towards water splitting reaction, was investigated in a photo-electrochemical cell in the presence of 0.1 M KOH electrolyte.

Table 3. Characteristics summary of the PEC-tested samples.

Label	Superficial treatment	PVA [%]	Glyc [g]	Ball milling [h]	Photocatalytic layer thickness
Ti-untr	none	4	11.01	4	22 ± 2 μm
Ti-tr	HCl 4h				23 ± 2 μm
Ti-11		2	11.01		11 ± 2 μm
Ti-9	HCl 4h			4	9 ± 2 μm
Ti-7		4	7.34		7 ± 1 μm
Ti-4					4 ± 1 μm

First of all, the effect of the applied surface treatment on the photoresponse was investigated. For this purpose, the behavior of two samples obtained with different surface treatments while using the same dispersion for coating was analyzed. In particular, one sample (thereafter denoted as Ti-untr) was just cleaned with acetone before being coated while the other (thereafter denoted as Ti-tr) was previously etched in HCl for 4 hours at 35 °C. For the sake of comparison, two samples with very similar thickness were considered. The results obtained over both samples in terms of photocurrent results and corresponding photoconversion efficiencies are shown in Fig. 7a and 7b,

respectively. For comparison purpose a typical result obtained under dark condition is also reported in Fig. 7a.
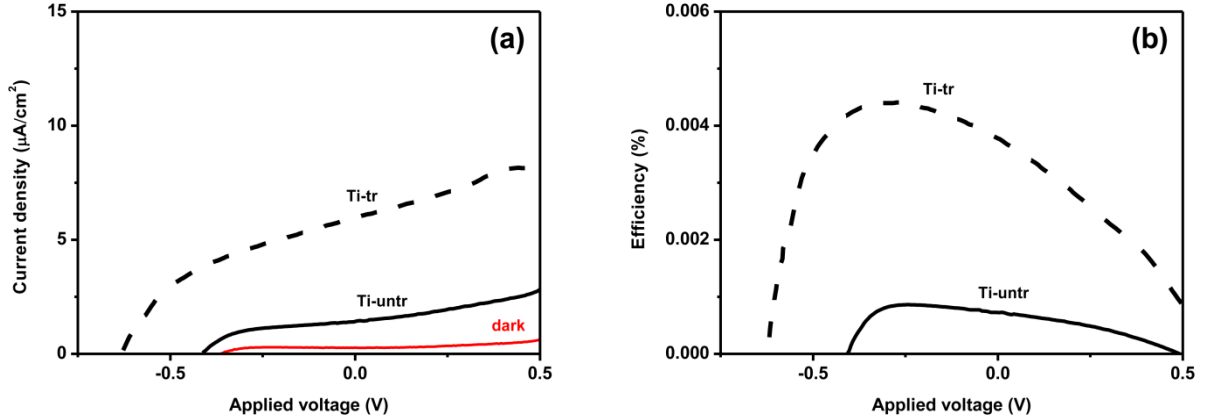

Fig. 7. (a) current density curves vs applied voltage, (b) efficiency of the two samples in function of the applied potential.

Of note, in the absence of light illumination, negligible photocurrent is observed over the whole investigated potential range (less than 1 $\mu A\ cm^{-2}$), indicating that no reaction occurred at the photoanodes under dark conditions. On the contrary, upon illumination, photocurrent generation is observed over both Ti-untr and Ti-tr samples, due to charge carriers (i.e. electron-holes pairs) generation from the incident light and the subsequent water oxidation at the photoanodes by holes. However, photocurrent curves are quite different in the two cases.

In the case of Ti-untr sample the photocurrent onset potential was observed near −0.41 V; then the photocurrent density gradually increased with the applied potential because of the increased charge carriers separation under the effect of the applied bias [48-50], finally reaching a near saturation condition, where the effect of the applied potential becomes less significant. However, very low photocurrent densities were measured through all the potential window in this case,

18

reaching values lower than 5 μA cm^{-2} at 0.5 V. Accordingly, very low photoconversion efficiencies were calculated, i.e. showing a maximum near 0.01 %.

Notably, the photoresponse increased for the Ti-tr sample. As a matter of fact the photocurrent onset was observed at a lower potential value (i.e. −0.63 V) and a saturated photocurrent density higher than 5 μA cm^{-2} was measured at 0.5 V. Accordingly, higher photoconversion efficiencies were obtained in this case, which suggests a more efficient generation, transfer of photogenerated charge carriers and minor recombination losses [51-53].

Accordingly, this indicates that the acid treatment had a positive effect on the photoanode performances. The reasons for this improvement can be found in the higher area of contact between the coating and the support (due to the increased roughness of the latter) and in the presence of a passive layer on top of the Ti, which could induce a stronger bonding of the semiconductor to the metallic slab.

On the basis of the above results, the effect of film thickness on the photoresponses was further investigated. For this purpose, the behavior of samples obtained with the same surface treatment but using different dispersion (i.e. resulting in different thickness) was analyzed. Fig. 8a and 8b show the photocurrent and the photoconversion efficiency results for samples with thickness of ca. 4, 7, 9 and 11 μm (thereafter denoted as Ti-4, Ti-7, Ti-9, Ti-11, respectively). For comparison purpose the results are also summarized in Table 4.
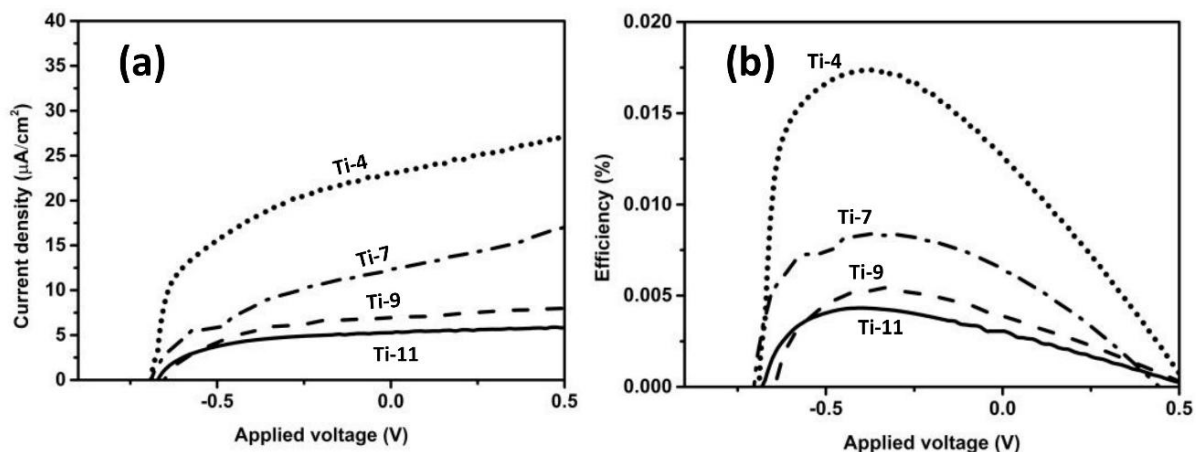
Fig. 8. Photocurrents (a) and efficiency (b) curves in function of the applied voltage. The reported samples are characterized by different oxide layer thicknesses.

As it clearly appears from Fig. 8a, the photocurrent onset is approximately the same (i.e., near −0.70 V) for all the samples; however, a clear effect of film thickness on the photoresponse is visible. The best performance was obtained with the Ti-4 sample (i.e. the thinnest sample), for which the highest photocurrent densities were measured in the whole potential window, i.e. reaching values near 30 μA cm^{-2} at 0.5 V. Accordingly, the highest photoconversion efficiency was measured in this case, i.e. near 0.018 % (Fig. 8b). Besides, upon moving from sample Ti-4 to sample Ti-11 (i.e. from ca. 4 to ca. 11 μm of thickness), the photoresponse was remarkably decreased. In particular, a photocurrent density of roughly 6μA cm^{-2} at 0.5 V was measured for sample Ti-11, which is ca. five times lower if compared to sample Ti-4. This was confirmed by the corresponding lower photoconversion efficiency (i.e. near 0.004 %).

Table 4. Photoelectrochemical properties of samples showing a different oxide layer thickness.

Sample	Ti-11	Ti-9	Ti-7	Ti-4
Thickness [μm]	11 ± 2	9 ± 2	7 ± 1	4 ± 1
Max photocurrent density [$\mu A/cm^2$]	6 ± 1	8 ± 1	17 ± 1	28 ± 1
Max efficiency [%]	0.004	0.006	0.009	0.018

The above results indicate a strong dependence of the photoelectrochemical performances on sample thickness, at least in the investigated range of thickness. This clearly appears from Fig. 9, where the photocurrent densities at 0.5 V and the maximum photocurrent efficiencies are shown as a function of the oxide layer thickness, respectively. Notably, a linear dependency is evident. A possible explanation to this trend can be found in the better adhesion and lower cracking of the thinner oxide layers. Thicker layers are less bonded to the conductor material, probably because the stresses generated during the coating consolidation may cause a partial detachment of the semiconductor near the cracks. Lower adhesion between Ti and TiO_2 is a symptom of an inefficient electrical contact between the photoanode constituents, which can lead to greater recombination at the interface and lower charge mobility.
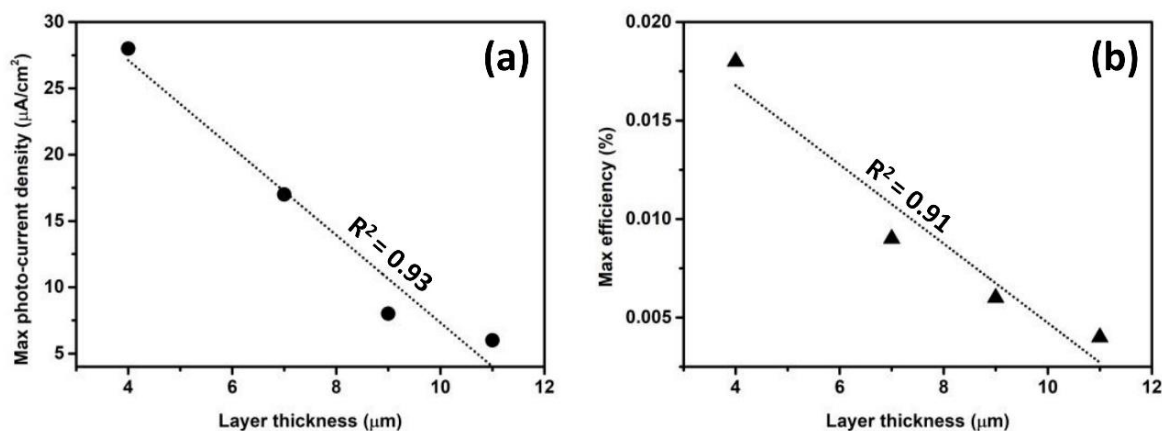
Fig. 9. Maximum photo-current density (a) and reached efficiency (b) as a function of the oxide layer thickness.

Besides, several works on TiO_2-based materials reported a strong correlation between film thickness and photo-response pointing out the existence of an optimum thickness value as a result of an optimal balance between charge carrier lifetime and light absorption [5, 54-56]. These results can be also considered as a starting point for future investigations on photoanodes produced with this technique, approaching lower oxide layer thicknesses.

4. Conclusions

TiO_2 layers deposition was performed on titanium slabs upon treatment in HCl. Such a treatment was able to increase metal surface roughness and to enhance the adhesion between the metal slab and the coated oxide film. This had a relevant effect on the photoelectrochemical properties, as the treated samples showed better photocatalytic performances during the tests.

Starting from a recipe developed in a previous work, which implies the use of polyvinyl alcohol and glycerol, the TiO_2 powder was dispersed in water solution. Moreover, a tuning of the slurry

formulation was made to achieve lower viscosities at a shear rate of 10 s^{-1} (a reference shear rate for the dip-coating technique). The samples coated with the less viscous slurry were the ones with the thinner resulting oxide layers.

The quality of the coating, in terms of percentage of area occupied by the crevices was assessed by SEM images of the coating surface. The thinner oxide layers showed a lower extent of the cracking phenomena, which was reflected in better endurance during the adhesion tests.

During the photo-electrochemical tests, the effect of the acid treatment on the performances was investigated and it was found that the treated sample performed much better than the untreated one in terms of efficiency. The effect of thickness on the photo-electrochemical efficiencies was also analyzed, achieving, for the photoanode showing the thinnest coating ($\approx$ 4 μm), an efficiency nearly 5 times larger than the one registered for the thickest one. This result could be explained by a better adhesion and electrical contact between the oxide layer and the metallic substrate when reducing coating thickness.

References

[1] U. S. E. I. A. (EIA), International Energy Outlook, 2017.

[2] S. Dutta, A review on production, storage of hydrogen and its utilization as an energy resource, J. Ind. Eng. Chem. 20 (2014) 1148-1156.

[3] A. Fujishima, K. Honda, Electrochemical photolysis of water at a semiconductor electrode, Nature 238 (1972) 37-38.

[4] M. Gratzel, Photoelectrochemical cells, Nature 414 (2001) 338-344.

[5] R. Matarrese, I. Nova, A. Li Bassi, C. S. Casari, V. Russo, S. Palmas, Preparation and optimization of TiO_2 photoanodes fabricated by pulsed laser deposition for photoelectrochemical water splitting, J. Solid State Electrochem. 21 (2017) 3139-3154.

[6] H. Pan, Principles on design and fabrication of nanomaterials as photocatalysts for water-splitting, Renew. Sust. Energ. Rev. 57 (2016) 584-601.

[7] H. J. Lewerenz, L. Peter, Photoelectrochemical water splitting: materials, processes and architectures, RSC Publishing, 2013.

[8] W.-T. Qiu, Y.-C. Huang, Z.-L.Wang, S. Xiao, H.-B. Ji, Y.-X. Tong, Effective Strategies towards High-Performance Photoanodes for Photoelectrochemical Water Splitting, Acta Phys.-Chim. Sin. 33(1) (2017) 80-102.

[9] X. Chen, S. Shen, L. Guo, S. S. Mao, Semiconductor-based Photocatalytic Hydrogen Generation, Chem. Rev. 110 (2010) 6503-6570.

[10] S. Yin, Y. Aita, M. Komatsu, T. Sato, Visible-light-induced photocatalytic activity of TiO_2-xNy prepared by solvothermal process in urea-alcohol system, J. Eur. Ceram. Soc. 26 (2006) 2735-2742.

[11] L. Youssef, A.J. Kinfack Leoga, S. Roualdes, J. Bassil, M. Zakhour, V. Rouessac, A. Ayral, M. Nakhl, Optimization of N-doped TiO_2 multifunctional thin layers by low frequency PECVD process, J. Eur. Ceram. Soc. 37 (2017) 5289-5303.

[12] I. Ganesh, A.K. Gupta, P.P. Kumar, P.S.C. Sekhar, K. Radha, G. Padmanabham, G. Sundararajan, Preparation and characterization of Co-doped TiO_2 materials for solar light induced current and photocatalytic applications, Mater. Chem. Phys. 135 (2012) 220-234.

[13] M.S. Mahmoud, E. Ahmed, A.A. Farghali, A.H. Zaki, N.A.M. Barakat, Synthesis of Fe/Co-doped titanate nanotube as redox catalyst for photon-induced water splitting, Mater. Chem. Phys. 217 (2018) 125-132.

[14] J.C. Chou, M.H. Yang, J.W. Liao, C.Y. Lee, J.Y. Gan, Photoexcitation of TiO_2 photoanode in water splitting, Mater. Chem. Phys. 143 (2014) 1417-1422.

[15] V. Kurnaravel, S. Mathew, J. Bartlett, S. C. Pillai, Photocatalytic hydrogen production using metal doped TiO_2: a review of recent advances, Appl. Catal. B-Environ. 244 (2019) 1021-1064.

[16] Y. J. Lin, G. B. Yuan, R. Liu, S. Zhou, S. W. Sheehan, D. W. Wang, Semiconductor nanostructure-based photoelectrochemical water splitting: a brief review, Chem. Phys. Lett. 507 (2011) 209-215.

[17] Z. Weng, H. Guo, X. Liu, S. Wu, K. W. K. Yeung, P. K. Chu, Nanostructured TiO_2 for energy conversion and storage, RSC Adv. 3 (2013) 24758-24775.

[18] S. Cabanas-Polo, A.R. Boccaccini, Electrophoretic deposition of nanoscale TiO_2: Technology and applications, J. Eur. Ceram. Soc. 36 (2016) 265-283.

[19] J. Domaradzki, D. Kaczmarek, E. L. Prociow, A. Borkowska, D. Schmeisser, G. Beuckert, Microstructure and optical properties of TiO_2 thin films prepared by low pressure hot target reactive magnetron sputtering, Thin Solid Films 513 (2006) 269-274.

[20] Y. Matsuura, F. Yoshii, T. Otsuka, K. Kadowaki, M. Ijiri, Y. Takemoto, K. Terashima, T. Wakita, T. Yokoya, Y. Muraoka, Multilayer formation via spinodal decomposition in TiO_2-VO_2 epitaxial films on sapphire substrates, J. Eur. Ceram. Soc. 38 (2018) 5043-5050.

[21] B.-H. Moon, Y.-M. Sung, C.-H. Han, Titanium oxide films prepared by sputtering, sol gel and dip coating methods for photovoltaic application, Energy Procedia 34 (2013) 589-596.

[22] H. Yu, S. Zhang, H. Zhao, G. Will, P. Liu, An efficient and low-cost TiO_2 compact layer for performance improvement of dye-sensitized solar cells, Electrochim. Acta 54 (2009) 1319-1324.

[23] L. Wu, D. Yang, L. Fei, Y. Huang, F. Wu, Y. Sun, J. Shi, Y. Xiang, Dip-coating process engineering and performance optimization for three-state electrochromic devices, Nanoscale Res. Lett. 12 (2017) 390.

[24] R. Subasri, M. Tripathi, K. Murugan, J. Revathi, G. V. N. Rao, T. N. Rao, Investigations on the photocatalytic activity of sol-gel derived plain and Fe^{3+}/Nb^{5+}-doped titania coatings on glass substrates, Mater. Chem. Phys. 124 (2010) 63-68.

[25] X. F. Wang, F. S. Han, X. F. Wang, Y. J. Li, Effect of aluminum foam support and polyethylene glycol on surface morphology and photocatalytic behavior of TiO_2 films, Mater. Chem. Phys. 145 (2014) 68-74.

[26] M. Mahé, J.-M. Heintz, J. Rödel, P. Reynders, Cracking of titania nanocrystalline coatings, J. Eur. Ceram. Soc. 28 (2008) 2003-2010.

[27] R. Ashiri, A. Nemati, M. Sasani Ghamsari, Crack-free nanostructured $BaTiO_3$ thin films prepared by sol–gel dip-coating technique, Ceram. Int. 40 (2014) 8613-8619.

[28] M. Bockmeyer, P. Löbmann, Crack formation in TiO_2 films prepared by sol–gel processing: quantification and characterization, Thin Solid Films 515 (2007) 5212-5219.

[29] M. Valentini, G. Groppi, C. Cristiani, M. Levi, E. Tronconi, P. Forzatti, The deposition of γ-Al_2O_3 layers on ceramic and metallic supports for the preparation of structured catalysts, Catal. Today 69 (2001) 307-314.

[30] C. Italiano, R. Balzarotti, A. Vita, S. Latorrata, C. Fabiano, L. Pino, C. Cristiani, Preparation of structured catalysts with Ni and Ni–Rh/CeO_2 catalytic layers for syngas production by biogas reforming processes, Catal. Today 273 (2016) 3-11.

[31] Y. Gu, C. Q. Xia, F. H. Zeng, C. B. Liu, Stabilized dispersion of nano-ceramic coating, T. Nonferr. Metal. Soc. 13 (2003) 890-892.

[32] C. Cristiani, E. Finocchio, S. Latorrata, C. G. Visconti, E. Bianchi, E. Tronconi, G. Groppi, P. Pollesel, Activation of metallic open-cell foams via washcoat deposition of Ni/$MgAl_2O_4$ catalysts for steam reforming reaction, Catal. Today 197 (2012) 256-264.

[33] S. Palmas, A. Da Pozzo, M. Mascia, A. Vacca, R. Matarrese, I. Nova, Photo-electrochemical behavior at different wavelengths of electrochemically obtained TiO_2 nanotubes, J. Appl. Electrochem. 42 (2012) 745-751.

[34] S. Palmas, A. Da Pozzo, M. Mascia, A. Vacca, A. Ardu, R. Matarrese, I. Nova, Effect of the preparation conditions on the performance of TiO_2 nanotube arrays obtained by electrochemical oxidation, Int. J. Hydrog. Energy 36 (2011) 8894-8901.

[35] J. Liu, X. L. Yu, Q. Y. Liu, R. J. Liu, X. K. Shang, S. S. Zhang, W. H. Li, W. Q. Zheng, G. J. Zhang, H. B. Cao, Z. J. Gu, Surface-phase junctions of branched TiO_2 nanorod arrays for efficient photoelectrochemical water splitting, Appl. Catal. B-Environ. 158 (2014) 296-300.

[36] O. K. Varghese, C. A. Grimes, Appropriate strategies for determining the photoconversion efficiency of water photo electrolysis cells: a review with examples using titania nanotube array photoanodes, Sol. Energ. Mat. Sol. C 92 (2008) 374-384.

[37] S. U. M. Khan, M. Al-Shahry, W. B. Ingler, Efficient photochemical water splitting by a chemically modified n-TiO$_2$ 2, Science 297 (2002) 2243-2245.

[38] M. D. M. Bruno Ramos Chrcanovic, Study of the influence of acid etching treatments on the superficial characteristics of Ti, Mater. Res. 17 (2) (2014) 373-380.

[39] A. I. H. Committee, ASM Handbook, ASM International, 2005.

[40] A. Trenczek-Zajac, Influence of etching on structural, optical and photoelectrochemical properties of titanium oxides obtained via thermal oxidation, Mat. Sci. Semicon. Proc. 83 (2018) 159-170.

[41] R. Balzarotti, C. Cristiani, S. Latorrata, A. Migliavacca, Washcoating of low surface area cerium oxide on complex geometry substrates, Particul. Sci. Technol. 34 (2016) 184-193.

[42] S. Middleman, Fundamentals of polymer processing, McGraw-Hill, New York, 1977.

[43] L.D. Landau, V.G. Levich, Entrainment of fluid by the driven plate, Acta Phys. Chim. 17 (1942) 42-54.

[44] C. Cristiani, M. Valentini, M. Merazzi, S. Neglia, P. Forzatti, Effect of ageing time on chemical and rheological evolution in γ-Al$_2$O$_3$ slurries for dip-coating, Catal. Today 105 (2005) 492-498.

[45] P. Xu, A. S. Mujumdar, B. Yu, Drying-induced cracks in thin film fabricated from colloidal dispersions, Dry. Technol. 27 (2009) 636-652.

[46] E. Santanach Carreras, F. Chabert, D. E. Dunstan, G. V. Franks, Avoiding "mud" cracks during drying of thin films from aqueous colloidal suspensions, J. Colloid. Interface Sci. 313 (2007) 160-168.

[47] L. A. Brown, C. F. Zukoski, L. R. White, Consolidation during drying of aggregated suspensions, AIChE J. 48 (2002) 492-502.

[48] F. Spadavecchia, S. Ardizzone, G. Cappelletti, L. Falciola, M. Ceotto, D. Lotti, Investigation and optimization of photocurrent transient measurements on nano-TiO_2, J.Appl. Electrochem. 43 (2013) 217-225.

[49] A. J. Cowan, J. W. Tang, W. H. Leng, J. R. Durrant, D. R. Klug, Water splitting by nanocrystalline TiO_2 in a complete photoelectrochemical cell exhibits efficiencies limited by charge recombination, J.Phys. Chem. C 114 (2010) 4208-4214.

[50] B. Zhou, M. Schulz, H. Y. Lin, S. I. Shah, J. H. Qu, C. P. Huang, Photoeletrochemical generation of hydrogen over carbon-doped TiO_2 photoanode, Appl. Catal. B-Environ. 92 (2009) 41-49.

[51] K. Zhang, X. J. Shi, J. K. Kim, J. H. Park, Photoelectrochemical cells with tungsten trioxide/Mo-doped $BiVO_4$ bilayers, Phys. Chem. Chem. Phys. 14 (2012) 11119-11124.

[52] Z. H. Xu, J. G. Yu, Visible-light-induced photoelectrochemical behaviors of Fe-modified TiO_2 nanotube arrays, Nanoscale 3 (2011) 3138-3144.

[53] X. M. Song, J. M. Wu, M. Z. Tang, B. Qi, M. Yan, Enhanced photoelectrochemical response of a composite titania thin film with single-crystalline rutile nanorods embedded in anatase aggregates, J. Phys. Chem. C 112 (2008) 19484-19492.

[54] J. M. Macak, H. Tsuchiya, A. Ghicov, K. Yasuda, R. Hahn, S. Bauer, P. Schmuki, TiO_2 nanotubes: self-organized electrochemical formation, properties and applications, Curr. Opin. Solid St. M. 11 (2007) 3-18.

[55] P. Aurora, P. Rhee, L. Thompson, Titania nanotube supported gold photoanodes for photoelectrochemical cells, J. Electrochem. Soc. 157 (2010) K152-K155.

[56] M. Altomare, K. Lee, M. S. Killian, E. Selli, P. Schmuki, Ta-doped TiO_2 nanotubes for enhanced solar-light photoelectrochemical water splitting, Chem.-Eur. J. 19 (2013) 5841-5844.